

Fluid-Solid Pattern Formation and Strain Localisation via Shear Banding Instability in Model Biological Tissues

Aidan J. Nicholas and Suzanne M. Fielding
*Department of Physics, Durham University, Science Laboratories,
 South Road, Durham DH1 3LE, United Kingdom.*

(Dated: March 10, 2026)

The rheological properties of biological tissues are core to processes such as cancer metastasis, wound healing and embryo development. The emergence of tissue and organ structures during morphogenesis requires the precise formation of spatial patterns. Dating back to Turing, pattern formation has been suggested to arise in tissues via spontaneous symmetry breaking instabilities in the concentration field of chemical morphogens. Within the vertex model of tissue mechanics, we show that spontaneous symmetry breaking may also arise via a mechanical instability in the strain field of a deformed tissue, leading to a patterned coexistence of fluid and solid regions, with a strong localisation of the strain into shear bands. The nature of the bands differs between tissues in which internal cell-cell dissipation dominates external drag against a substrate, and vice versa.

Biological tissues display a host of rheological (deformation and flow) phenomena that are key to processes such as embryo development, tumour progression and wound healing. They are viscoelastic [1], behaving as deformable solids on short timescales [2] but also showing power law stress relaxation [3] and slowly reshaping via internally active processes that include cell rearrangements, division and death [4–6]. In nonlinear deformation they display strain stiffening [7]. Tissues can also fracture [8] as a result of externally imposed stretching [7] or an organism’s own internally generated motility [9].

The emergence of tissue and organ structures during morphogenesis [10–12], for example in gastrulation and neural tube formation, requires the formation of precise spatial patterns. Turing suggested that patterning may arise in tissues via spontaneous symmetry breaking instabilities in the spatio-temporal reaction-diffusion dynamics of chemical morphogens [13, 14]. Crick put forward a scaling argument to suggest that diffusion may be responsible for establishing morphogen gradients [15].

Beyond purely chemical morphogenetic patterning, considerable attention also concerns the role of mechanics [10–12, 16–22]. For a tissue to reshape itself requires the concerted motion of groups of cells, and tissues experience external stresses, as well as active stresses generated internally by actin-myosin networks and transmitted over long length-scales [23]. Tissues also show spontaneous solid-fluid jamming-unjamming transitions (and vice versa) [24–27], often linked to changes in cell shape [25, 28], and sometimes with a coexistence of fluid and solid regions [29]. A stress-induced fluidisation transition has also been observed [30]. Imaging techniques that track cell trajectories [31] show that the strain field within a tissue can be heterogeneous, with localised strains [5, 9, 32]. The concept of Lagrangian coherent structures [33], used to study flow patterns in fluid mechanics, has been adapted to analyse attracting and repelling organisers of cell trajectories [34]. It is therefore natural to ask to what extent mechanical instabili-

ties contribute to pattern formation in tissues, alongside, and potentially interacting with, chemical instabilities.

The mechanics of a tissue is governed not only by elastic stresses, but also by frictional drag stemming from the breakage and reformation of cell adhesions. This is often modeled as viscous dissipation [35, 36], assuming tissue reshaping to be slow in comparison. It can arise internally within a tissue, via cell-cell adhesions, and externally via adhesive contacts between a tissue monolayer and a supporting substrate. Reducing internal cell-cell adhesions reduced the correlation length of cooperative cell motions in Ref. [37]. Increasing external substrate stiffness increased the correlation length in Ref. [38]. Tissue reshaping can also occur without any supporting substrate, e.g. during gastrulation in early embryo development. Actively driven global flows emerged spontaneously in a theoretical model of active tissues with internal cell-cell dissipation in Ref. [39], but were suppressed by external cell-substrate dissipation.

In this Letter, we show that a patterned coexistence of fluid and solid regions can arise via spontaneous symmetry breaking in a model biological tissue subject to an imposed deformation. It does so via a mechanical shear banding instability that occurs as the tissue yields from an initially solid-like. The strain becomes strongly localised in the high shear band(s), with other parts of the sample behaving elastically in comparison. The bands can persist on long timescales, before healing towards a homogeneously fluidised state. The nature of the bands depends strongly on the form of viscous drag. With internal cell-cell dissipation, a single shear band forms, of width set by the system size. With external cell-substrate dissipation, multiple smaller bands can form.

We work within the widely studied vertex model of tissue mechanics [40–42]. However, shear bands arise commonly when soft solids yield [43–51] suggesting that our findings may be independent of model and deformation protocol (unidirectional vs oscillatory strain, imposed strain vs. imposed stress, etc.).

Vertex model — A tissue monolayer of confluent packed cells is modeled as a 2D tiling of $c = 1 \dots C$ polygons, with each cell defined by the location of its $n_c = 1 \dots N_c$ vertices. The tissue's elastic energy [20, 41]

$$E = \frac{1}{2} \sum_{c=1}^C [\kappa_A (A_c - A_{c0})^2 + \kappa_P (P_c - P_{c0})^2]. \quad (1)$$

The first term on the RHS models cell volume incompressibility in 3D (considering the monolayer's height) by means of an effective 2D area elasticity, with an energy cost when any cell's area A_c differs from a target A_{c0} . The second term models cell-edge tension, with an energy cost when any cell's perimeter P_c differs from a target P_{c0} , governed by a competition between cell cortical contractility and cell-cell adhesion. The area and perimeter stiffnesses κ_A and κ_P are assumed the same for all cells in the tissue, as is the target cell shape $p_0 = P_{c0}/\sqrt{A_{c0}}$.

The tissue's dynamics is governed by the interplay between the resulting elastic forces, with force $\vec{F}_n = -\frac{\delta E}{\delta \vec{x}_n}$ on the n th vertex, and viscous dissipation, which we prescribe below. We also allow plasticity [52, 53] via T1 cell rearrangements: when the edge connecting any two neighbouring vertices shrinks below a small length l_c , these two original vertices (at the junction of cells $\alpha\beta\gamma$ and $\alpha\beta\delta$, say) are replaced by new ones at the junctions of cells $\beta\gamma\delta$ and $\alpha\gamma\delta$, giving cell neighbour exchange.

A key finding in what follows will be that the yielding of biological tissues, as predicted by the vertex model, depends strongly on the type of dissipation a tissue experiences. We study two different forms of dissipation. First, we consider dissipation dominated by drag of the constituent cells against an external substrate. Here the position \vec{x}_n of the n th vertex moves with velocity:

$$\vec{v}_n \equiv \frac{d\vec{x}_n}{dt} = \zeta^{-1} \vec{F}_n, \quad (2)$$

with drag coefficient ζ . Second, for a tissue monolayer in which any external substrate drag is negligible compared with in-plane drag impeding relative motion of neighbouring vertices internally within the tissue, we have [39]

$$\sum_{m \in S_n} (\vec{v}_n - \vec{v}_m) = \xi^{-1} \vec{F}_n. \quad (3)$$

Alternatively, we can think of this model with internal drag as a simplified 2D projection of a bulk 3D tissue. The sum in Eqn. 3 runs over all neighbouring vertices m of any vertex n . For the tissue as a whole this gives a linear system $M \cdot V = \zeta^{-1} F$ in the vectors V and F of vertex velocities and forces. Each row of the sparse matrix M has +3 on the diagonal and three -1 entries at locations determined by the vertex neighbour connectivities, updated after each T1 event. Applying Eqn. 3 to every vertex would render M singular, due to Galilean invariance. Choosing a reference frame modifies one line

of the linear system, lifting this degeneracy. The system's centre of mass velocity is zero in all the results presented.

Protocol — We initialise a square Voronoi tiling of polygons [54], render it biperiodic using the algorithm of Ref. [55], then evolve the tissue to equilibrium for any target cell shape p_0 , taking RMS vertex velocity $< 10^{-8}$ as our criterion for equilibrium. In equilibrium, the vertex model shows a transition at a critical $p_0 = p_0^*$ [56–58]. For $p_0 < p_0^*$ it behaves as a solid with finite linear shear modulus. For $p_0 > p_0^*$ it is floppy in linear response, with no resistance to small shear deformations, but stiffens beyond a finite imposed strain, $\gamma > \gamma^*(p_0)$ [59].

At time $t = 0$, we switch on a shear strain of rate $\dot{\gamma}$, with flow direction x and shear gradient y , and Lees-Edwards periodic boundary conditions [60]. In a tissue with external dissipation, vertex n then moves as $\vec{v}_n = \zeta^{-1} \vec{F}_n + \dot{\gamma} y_n \vec{x}$, with a shear term added to Eqn. 2. With internal dissipation, co-sliding of the stacked periodic boxes is implemented via a velocity source vector \vec{G} with entries $\dot{\gamma} L_y$ (resp. $-\dot{\gamma} L_y$) for any vertex whose connector to its neighbour crosses the domain's top (resp. bottom) boundary, giving the modified system $M \vec{V} = \xi^{-1} \vec{F} + \vec{G}$, counterpart to Eqn. 3. This shear communicates across the tissue via the drag between neighbouring vertices.

Parameters — We simulate a 50 : 50 bidisperse tiling of C cells of target areas $A_0 = 1, 1.4$, which sets our unit of length, and use units of modulus and time in which $\kappa_A = 1$ and $\zeta = 1$. We choose $\kappa_p = 1.0$. Our numerical timestep $\Delta t = 0.01$ and the threshold for T1 events $l_c = 0.02$. Parameters to vary will be the target cell shape p_0 , imposed shear rate $\dot{\gamma}$ and system size C .

Results — In exploring yielding as a function of time t or (essentially equivalently) imposed strain $\gamma = \dot{\gamma} t$ since the inception of shear of constant rate $\dot{\gamma}$, we shall report the global stress-strain curve $\Sigma(\gamma)$, with Σ the xy component of the stress tensor $\Sigma_{ij}(t) = \frac{1}{N_c} \sum_{n=1}^{N_c} F_{ni} x_{nj}$, where the sum runs over all vertices in the tiling. We shall also study the way in which the strain field within the tissue becomes localised into shear bands with layer normals in the gradient direction y , and quantify this shear banding using measures to be defined below.

Figs. 1(a+b) show the global stress-strain curves for a tissue with internal and external dissipation respectively. In each case, the stress initially rises almost linearly with imposed strain, signifying near elastic response. It then attains a maximum, beyond which the tissue yields and the stress decreases to a constant, signifying a state of plastic flow. With external dissipation, the decrease in stress during yielding happens in a smooth and gradual way. With internal dissipation, the decrease is relatively smooth for small system sizes, but becomes progressively more precipitous for larger systems.

Panels 1g-l) show density maps of the number of plastic T1 rearrangement events that arise as a function of

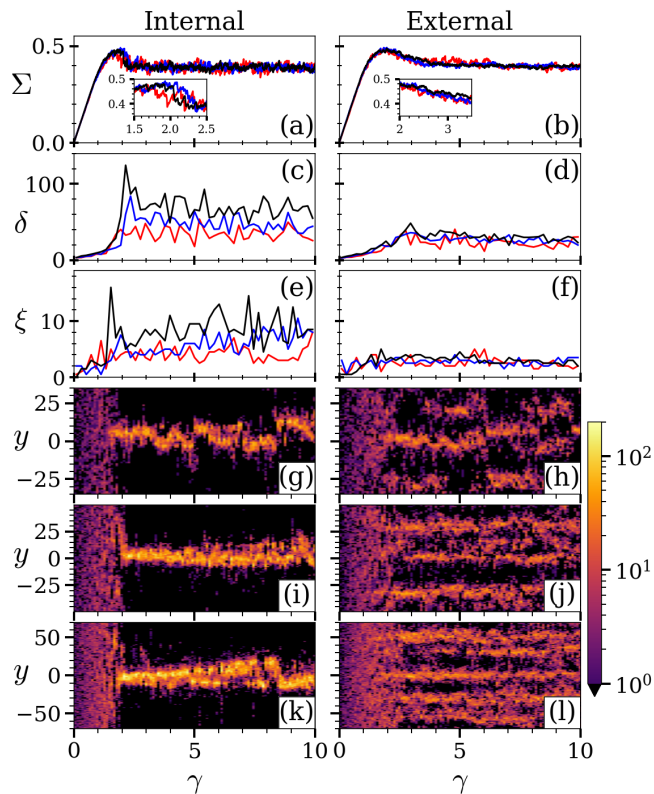


FIG. 1. Yielding phenomenology of the vertex model with internal dissipation (left) and external dissipation (right). Shown as a function of strain γ are the stress Σ (a+b), standard deviation of plasticity δ (c+d), and correlation length ξ (e+f), with δ and ξ defined in the main text. System sizes $C = 4096, 8192, 16384$ in red, blue and black curves respectively. Data in (c-f) are averaged over strain bins of size $\Delta\gamma = 0.2$. Distribution of T1 events across the flow-gradient direction y versus strain γ (in a single realisation, binned over $\Delta\gamma = 0.1$ and $\Delta y = 1$) for $C = 4096$ (g+h), $C = 8192$ (i+j) and $C = 16384$ (k+l). No T1 events arise in black regions. $p_0 = 3.5$, $\dot{\gamma} = 10^{-4}$.

imposed strain γ , spatially resolved across the flow gradient direction y . At short times (small strains) plastic events are rare, and any that do arise are distributed essentially uniformly across y . A major change then occurs as the tissue yields. The plastic events become much more numerous and furthermore organise into a spatially localised band (or bands), with layer normals along y . (The y -origin is chosen to coincide the y -bin in which the most T1 events occur for $0 < \gamma < 10$.) In no case did we observe localisation along x . Because each plastic event leads to an additional forward plastic strain, beyond the globally imposed one, any band of high plasticity is also one of strong shear. The shear rate integrated across y must however remain equal to the globally imposed one. Accordingly, outwith the plastic bands the shear rate is lower than the imposed rate. Here the tissue deforms essentially elastically, with no plastic events.

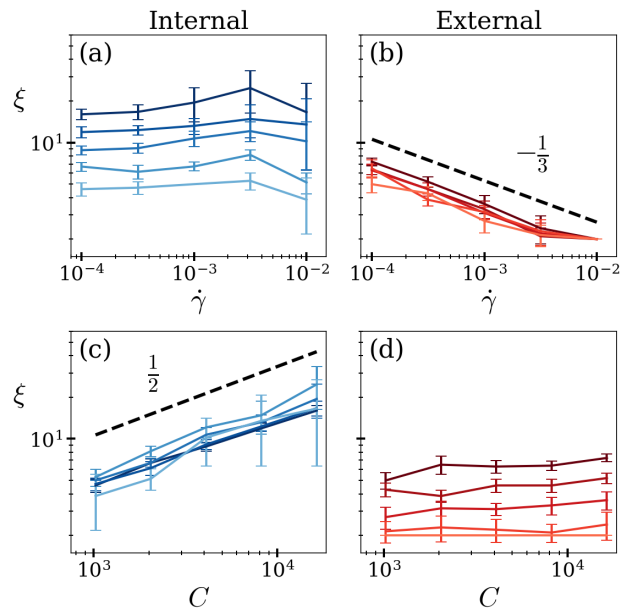


FIG. 2. Correlation length with internal dissipation (a+c) and external dissipation (b+d), as a function of shear rate for system sizes $C = 1024, 2048, \dots, 16384$ increasing in curves from light to dark (a+b), and as a function of system size for shear rates $\dot{\gamma} = 10^{-n}$ with $n = 0.0, -0.5, \dots, -4.0$, the shear rate decreasing in curves from light to dark (c+d). Data averaged over the strain interval $2.0 < \gamma < 6.0$ and over 10 realisations. Dashed lines show power laws indicated, as a guide to the eye. Shape parameter $p_0 = 3.5$.

Comparing the left and right columns of Fig. 1 reveals a qualitative difference in the nature of the bands in tissues with internal versus external dissipation. With internal dissipation, a single macroscopic band develops, of a size that increases with system size in (g) to (k) downwards. With external dissipation, multiple narrow bands develop, which increase in number at roughly fixed band width as the system size increases in (h) to (l) downwards.

We now define two measures to quantify the banding, as evolving functions of the imposed strain γ . During each strain increment $\gamma \rightarrow \gamma + \Delta\gamma$, with $\Delta\gamma = 0.1$, we divide the y axis into bins of size $\Delta y = 1.0$, and count the number of T1 events that occur in each bin. The standard deviation $\delta(\gamma)$ in this number across y then measures how strongly the plasticity (and so strain rate) is banded across y . The extent $C(\Delta y)$ to which the number of plastic events at any y is correlated with that at $y + \Delta y$, in any strain increment $\gamma \rightarrow \gamma + \Delta\gamma$, further defines a correlation length $\xi(\gamma)$, via the value of Δy at which this correlation function $C(\Delta y)$ falls to zero. Accordingly, the evolving standard deviation $\delta(\gamma)$ measures the evolving *amplitude* of shear banding and the correlation length $\xi(\gamma)$ the characteristic *width* of the bands.

At early times (small strains), the standard deviation $\delta(\gamma)$ is small (Figs. 1c+d), consistent with near uniform shear. It then rises dramatically as shear bands form.

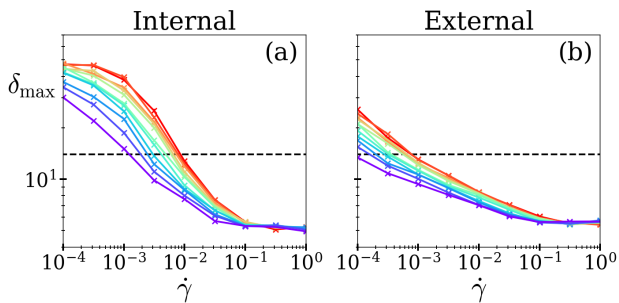


FIG. 3. Amplitude of shear banding in the vertex model with (a) internal dissipation and (b) external dissipation. The amplitude is quantified by the standard deviation δ_{\max} defined in the main text, plotted as a function of shear rate for values of the shape parameter $p_0 = 3.50, 3.55, \dots, 4.00$ in curves red, orange \dots purple. Data averaged over 10 realisations. System size $C = 8192$. In snapshots of the kind shown in Fig. 1g-l) and 4c-f), shear bands are visually apparent for values of δ_{\max} above the dashed line.

With external dissipation, the standard deviation and correlation length (panels d+f) are almost independent of system size, consistent with a spatial pattern of bands that remains statistically comparable in any macroscopic slice of the system of a given height in y , as the system size increases in panels h) to l) downwards. In contrast, with internal dissipation both measures increase with increasing system size (panels c+e), consistent with the formation of a single band that is broader in larger systems from g) to k) downwards.

Fig. 2 explores this dependence in more detail. With internal dissipation, the correlation length grows with system size as $\xi \sim C^m$ with $m = 0.47 \pm 0.02$ (panel c), suggesting that $\xi \sim C^{1/2} \sim L_y$ where $L_y \propto \sqrt{C}$ is the height of our square simulation box, consistent with a single band of width that grows with system size. Recall Figs. 1g) to k) downwards. ξ is however relatively independent of shear rate, in this case of internal dissipation (panel a). With external dissipation the correlation length is relatively independent of system size (panel d), consistent with the formation of an increasing number of bands of roughly constant band width as system size increases in Figs. 1 h) to l) downwards. The band width however increases with decreasing shear rate, $\xi \sim \dot{\gamma}^{-p}$ with $p \approx 0.30 \pm 0.02$ (panel b).

So far, we have considered a fixed value of the target cell shape in the regime for which the tissue is solid in linear response, $p_0 = 3.5 < p_0^*$. The phenomenology we report is however qualitatively robust to changing p_0 . To evidence this, we quantify the amplitude of shear banding across a full range of p_0 (and shear rate $\dot{\gamma}$) via the standard deviation $\delta(\dot{\gamma})$ defined above. For any p_0 and $\dot{\gamma}$, we further maximise δ over the strain interval $1.5 < \gamma < 4.0$ during which shear bands form, when δ indeed peaks as seen in Fig. 1c+d). This maximum δ_{\max} is reported in

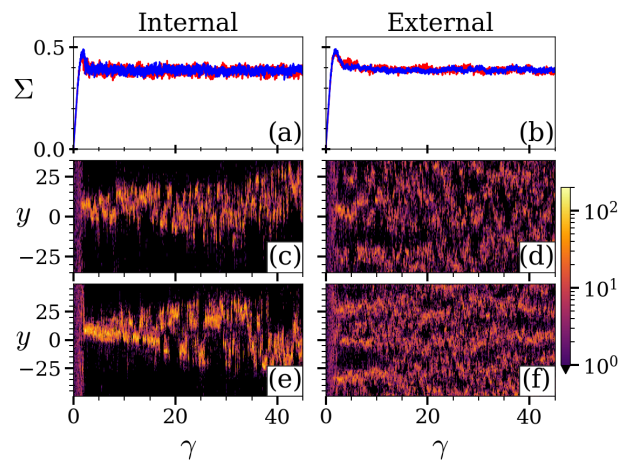


FIG. 4. Curves as in Fig. 1 (a+b) and (g-j), but now over the larger strain interval $0 < \gamma < 45$ to show the evolution of the shear bands at long times and large strains.

Fig. 3 as a function of shear rate for a range of p_0 values, below and above p_0^* . In each case, δ_{\max} decreases with imposed shear rate. As noted above, for $p_0 > p_0^*$ the tissue is initially floppy in linear response but solidifies at modest imposed strains [59]. It then subsequently yields, and shear bands form as it does so.

We have shown, then, that the vertex model predicts the formation of shear bands as a tissue first yields from an initially solid state towards a plastically flowing one. Finally in Fig. 4 we explore the fate of the bands over longer timescales, as shearing continues to large strains. With internal dissipation (left panels), for which just a single band forms as the tissue first yields, the band progressively broadens over time. This suggests that the tissue may eventually become homogeneously fluidised at very long times, which are however inaccessible computationally, and indeed perhaps unlikely to arise in tissues. In a tissue with external dissipation, for which multiple smaller bands form during yielding, the pattern of banding appears to remain statistically relatively constant over the full duration accessible computationally. Whether the flow finally homogenises on even longer timescales remains an open question.

Conclusion — We have predicted that a mechanical shear banding instability arises in a model biological tissue during yielding from an initially solid-like state towards a plastically flowing state. This leads to a patterned coexistence of solid and fluidised regions, with a strong localisation of the imposed strain in the high shear band, the rest of the tissue behaving essentially elastically in comparison. We have shown the nature of the bands to depend strongly on the form of dissipation present: internal cell-cell vs external cell-substrate. It remains an open challenge to elucidate more fully the fate of the bands at longer times. It would be interesting to examine whether shear bands might also form in tissues during yielding un-

der imposed stress [48, 49] and oscillatory shear [50, 51], as in other soft solids.

Acknowledgements — This project has received funding from the European Research Council (ERC) under the European Union’s Horizon 2020 research and innovation programme (grant agreement No. 885146).

-
- [1] G. Forgacs, R. A. Foty, Y. Shafrir, and M. S. Steinberg, Viscoelastic properties of living embryonic tissues: a quantitative study, *Biophysical journal* **74**, 2227 (1998).
- [2] H. Phillips and M. Steinberg, Embryonic tissues as elasticoviscous liquids: I. rapid and slow shape changes in centrifuged cell aggregates, *Journal of cell science* **30**, 1 (1978).
- [3] N. Khalilgharibi, J. Fouchard, N. Asadipour, R. Barrientos, M. Duda, A. Bonfanti, A. Yonis, A. Harris, P. Mosaffa, Y. Fujita, *et al.*, Stress relaxation in epithelial monolayers is controlled by the actomyosin cortex, *Nature physics* **15**, 839 (2019).
- [4] B. Guirao, S. U. Rigaud, F. Bosveld, A. Bailles, J. Lopez-Gay, S. Ishihara, K. Sugimura, F. Graner, and Y. Bellaïche, Unified quantitative characterization of epithelial tissue development, *Elife* **4**, e08519 (2015).
- [5] R. Etournay, M. Popović, M. Merkel, A. Nandi, C. Blasse, B. Aigouy, H. Brandl, G. Myers, G. Salbreux, F. Jülicher, *et al.*, Interplay of cell dynamics and epithelial tension during morphogenesis of the drosophila pupal wing, *Elife* **4**, e07090 (2015).
- [6] T. Wyatt, B. Baum, and G. Charras, A question of time: tissue adaptation to mechanical forces, *Current opinion in cell biology* **38**, 68 (2016).
- [7] A. R. Harris, L. Peter, J. Bellis, B. Baum, A. J. Kabla, and G. T. Charras, Characterizing the mechanics of cultured cell monolayers, *Proceedings of the National Academy of Sciences* **109**, 16449 (2012).
- [8] A. Bonfanti, J. Duque, A. Kabla, and G. Charras, Fracture in living tissues, *Trends in Cell Biology* **32**, 537 (2022).
- [9] V. N. Prakash, M. S. Bull, and M. Prakash, Motility-induced fracture reveals a ductile-to-brittle crossover in a simple animal’s epithelia, *Nature Physics* **17**, 504 (2021).
- [10] K. Goodwin and C. M. Nelson, Mechanics of development, *Developmental cell* **56**, 240 (2021).
- [11] J. Sutlive, H. Xiu, Y. Chen, K. Gou, F. Xiong, M. Guo, and Z. Chen, Generation, transmission, and regulation of mechanical forces in embryonic morphogenesis, *Small* **18**, 2103466 (2022).
- [12] C.-P. Heisenberg and Y. Bellaïche, Forces in tissue morphogenesis and patterning, *Cell* **153**, 948 (2013).
- [13] A. Turing, The chemical basis of morphogenesis (1952), *B Jack Copeland* **519** (1952).
- [14] A. M. Turing, The chemical basis of morphogenesis, *Bulletin of mathematical biology* **52**, 153 (1990).
- [15] F. Crick, Diffusion in embryogenesis, *Nature* **225**, 420 (1970).
- [16] D. J. Montell, Morphogenetic cell movements: diversity from modular mechanical properties, *Science* **322**, 1502 (2008).
- [17] T. Lecuit and P.-F. Lenne, Cell surface mechanics and the control of cell shape, tissue patterns and morphogenesis, *Nature reviews Molecular cell biology* **8**, 633 (2007).
- [18] G. M. Odell, G. Oster, P. Alberch, and B. Burnside, The mechanical basis of morphogenesis: I. epithelial folding and invagination, *Developmental biology* **85**, 446 (1981).
- [19] M.-K. Hayward, J. M. Muncie, and V. M. Weaver, Tissue mechanics in stem cell fate, development, and cancer, *Developmental cell* **56**, 1833 (2021).
- [20] R. Farhadifar, J.-C. Röper, B. Aigouy, S. Eaton, and F. Jülicher, The influence of cell mechanics, cell-cell interactions, and proliferation on epithelial packing, *Current biology* **17**, 2095 (2007).
- [21] C. Villeneuve, A. Hashmi, I. Ylivinkka, E. Lawson-Keister, Y. A. Miroshnikova, C. Pérez-González, S.-M. Myllymäki, F. Bertillot, B. Yadav, T. Zhang, *et al.*, Mechanical forces across compartments coordinate cell shape and fate transitions to generate tissue architecture, *Nature Cell Biology* **26**, 207 (2024).
- [22] R. K. Manna, E. M. Retzlaff, A. M. Hinman, Y. Lan, O. Abdel-Razek, M. Bates, H. Hehnlly, J. D. Amack, and M. L. Manning, Dynamic forces drive cell and organ morphology changes during embryonic development, *Proceedings of the National Academy of Sciences* **122**, e241811122 (2025).
- [23] E. Sadeghipour, M. A. Garcia, W. J. Nelson, and B. L. Pruitt, Shear-induced damped oscillations in an epithelium depend on actomyosin contraction and e-cadherin cell adhesion, *Elife* **7**, e39640 (2018).
- [24] C. Malinverno, S. Corallino, F. Giavazzi, M. Bergert, Q. Li, M. Leoni, A. Disanza, E. Frittoli, A. Oldani, E. Martini, *et al.*, Endocytic reawakening of motility in jammed epithelia, *Nature materials* **16**, 587 (2017).
- [25] J.-A. Park, J. H. Kim, D. Bi, J. A. Mitchel, N. T. Qazvini, K. Tantisira, C. Y. Park, M. McGill, S.-H. Kim, B. Gweon, *et al.*, Unjamming and cell shape in the asthmatic airway epithelium, *Nature materials* **14**, 1040 (2015).
- [26] S. Garcia, E. Hannezo, J. Elgeti, J.-F. Joanny, P. Silberzan, and N. S. Gov, Physics of active jamming during collective cellular motion in a monolayer, *Proceedings of the National Academy of Sciences* **112**, 15314 (2015).
- [27] L. Oswald, S. Grosser, D. M. Smith, and J. A. Käs, Jamming transitions in cancer, *Journal of physics D: Applied physics* **50**, 483001 (2017).
- [28] L. Atia, D. Bi, Y. Sharma, J. A. Mitchel, B. Gweon, S. A. Koehler, S. J. DeCamp, B. Lan, J. H. Kim, R. Hirsch, *et al.*, Geometric constraints during epithelial jamming, *Nature physics* **14**, 613 (2018).
- [29] A. Mongera, P. Rowghanian, H. J. Gustafson, E. Shelton, D. A. Kealhofer, E. K. Carn, F. Serwane, A. A. Lucio, J. Giammona, and O. Campàs, A fluid-to-solid jamming transition underlies vertebrate body axis elongation, *Nature* **561**, 401 (2018).
- [30] G. Cai, A. Nguyen, Y. Bashirzadeh, S.-S. Lin, D. Bi, and A. P. Liu, Compressive stress drives adhesion-dependent unjamming transitions in breast cancer cell migration, *Frontiers in Cell and Developmental Biology* **10**, 933042 (2022).
- [31] P. J. Keller, Imaging morphogenesis: technological advances and biological insights, *Science* **340**, 1234168 (2013).
- [32] E. Latorre, S. Kale, L. Casares, M. Gómez-González, M. Uroz, L. Valon, R. V. Nair, E. Garreta, N. Montserrat, A. Del Campo, *et al.*, Active superelasticity in three-dimensional epithelia of controlled shape, *Nature* **563**,

- 203 (2018).
- [33] G. Haller, Lagrangian coherent structures, *Annual review of fluid mechanics* **47**, 137 (2015).
- [34] M. Serra, S. Streichan, M. Chuai, C. J. Weijer, and L. Mahadevan, Dynamic morphoskeletons in development, *Proceedings of the National Academy of Sciences* **117**, 11444 (2020).
- [35] S. Tong, N. K. Singh, R. Sknepnek, and A. Košmrlj, Linear viscoelastic properties of the vertex model for epithelial tissues, *PLoS computational biology* **18**, e1010135 (2022).
- [36] S. Tong, R. Sknepnek, and A. Košmrlj, Linear viscoelastic response of the vertex model with internal and external dissipation: Normal modes analysis, *Physical Review Research* **5**, 013143 (2023).
- [37] A. Czirók, K. Varga, E. Méhes, and A. Szabó, Collective cell streams in epithelial monolayers depend on cell adhesion, *New journal of physics* **15**, 075006 (2013).
- [38] K. Vazquez, A. Saraswathibhatla, and J. Notbohm, Effect of substrate stiffness on friction in collective cell migration, *Scientific Reports* **12**, 2474 (2022).
- [39] J. Rozman, K. Chaithanya, J. M. Yeomans, and R. Sknepnek, Vertex model with internal dissipation enables sustained flows, *Nature Communications* **16**, 530 (2025).
- [40] T. Nagai and H. Honda, A dynamic cell model for the formation of epithelial tissues, *Philosophical Magazine B* **81**, 699 (2001).
- [41] D. B. Staple, R. Farhadifar, J.-C. Röper, B. Aigouy, S. Eaton, and F. Jülicher, Mechanics and remodelling of cell packings in epithelia, *The European Physical Journal E* **33**, 117 (2010).
- [42] A. G. Fletcher, M. Osterfield, R. E. Baker, and S. Y. Shvartsman, Vertex models of epithelial morphogenesis, *Biophysical journal* **106**, 2291 (2014).
- [43] T. Divoux, D. Tamarii, C. Barentin, and S. Manneville, Transient shear banding in a simple yield stress fluid, *arXiv preprint arXiv:1003.0161* (2010).
- [44] J. D. Martin and Y. T. Hu, Transient and steady-state shear banding in aging soft glassy materials, *Soft Matter* **8**, 6940 (2012).
- [45] C. J. Dimitriou and G. H. McKinley, A comprehensive constitutive law for waxy crude oil: a thixotropic yield stress fluid, *Soft Matter* **10**, 6619 (2014).
- [46] S. M. Fielding, Triggers and signatures of shear banding in steady and time-dependent flows, *Journal of Rheology* **60**, 821 (2016).
- [47] M. L. Manning, J. S. Langer, and J. Carlson, Strain localization in a shear transformation zone model for amorphous solids, *Physical Review E—Statistical, Nonlinear, and Soft Matter Physics* **76**, 056106 (2007).
- [48] V. Grenard, T. Divoux, N. Taberlet, and S. Manneville, Timescales in creep and yielding of attractive gels, *Soft matter* **10**, 1555 (2014).
- [49] T. Sentjabrskaja, P. Chaudhuri, M. Hermes, W. Poon, J. Horbach, S. Egelhaaf, and M. Laurati, Creep and flow of glasses: Strain response linked to the spatial distribution of dynamical heterogeneities, *Scientific reports* **5**, 11884 (2015).
- [50] I. Cohen, B. Davidovitch, A. B. Schofield, M. P. Brenner, and D. A. Weitz, Slip, yield, and bands in colloidal crystals under oscillatory shear, *Physical review letters* **97**, 215502 (2006).
- [51] C. Perge, N. Taberlet, T. Gibaud, and S. Manneville, Time dependence in large amplitude oscillatory shear: A rheo-ultrasonic study of fatigue dynamics in a colloidal gel, *Journal of Rheology* **58**, 1331 (2014).
- [52] M. Popović, V. Druelle, N. A. Dye, F. Jülicher, and M. Wyart, Inferring the flow properties of epithelial tissues from their geometry, *New Journal of Physics* **23**, 033004 (2021).
- [53] A. Q. Nguyen, J. Huang, and D. Bi, Origin of yield stress and mechanical plasticity in model biological tissues, *Nature Communications* **16**, 3260 (2025).
- [54] G. Voronoi, Nouvelles applications des paramètres continus à la théorie des formes quadratiques. premier mémoire. sur quelques propriétés des formes quadratiques positives parfaites., *Journal für die reine und angewandte Mathematik (Crelles Journal)* **1908**, 97 (1908).
- [55] D.-M. Yan, K. Wang, B. Lévy, and L. Alonso, Computing 2d periodic centroidal voronoi tessellation, in *2011 eighth international symposium on Voronoi diagrams in science and engineering (IEEE, 2011)* pp. 177–184.
- [56] D. Bi, J. Lopez, J. M. Schwarz, and M. L. Manning, A density-independent rigidity transition in biological tissues, *Nature Physics* **11**, 1074 (2015).
- [57] D. Bi, X. Yang, M. C. Marchetti, and M. L. Manning, Motility-driven glass and jamming transitions in biological tissues, *Physical Review X* **6**, 021011 (2016).
- [58] M. Moshe, M. J. Bowick, and M. C. Marchetti, Geometric frustration and solid-solid transitions in model 2d tissue, *Physical review letters* **120**, 268105 (2018).
- [59] J. Huang, J. O. Cochran, S. M. Fielding, M. C. Marchetti, and D. Bi, Shear-driven solidification and non-linear elasticity in epithelial tissues, *Physical Review Letters* **128**, 178001 (2022).
- [60] A. W. Lees and S. F. Edwards, The computer study of transport processes under extreme conditions, *Journal of Physics C: Solid State Physics* **5**, 1921 (1972).